Optimizing the spatial resolution of photonic crystal label-free imaging

Ian D. Block,[1] Patrick C. Mathias,[2] Sarah I. Jones,[3]
Lila O. Vodkin,[3] and Brian T. Cunningham[1,*]

[1]Department of Electrical and Computer Engineering, University of Illinois at Urbana-Champaign, Urbana, Illinois, USA

[2]Department of Bioengineering, University of Illinois at Urbana-Champaign, Urbana, Illinois, USA

[3]Department of Crop Sciences, University of Illinois at Urbana-Champaign, Urbana, Illinois, USA

*Corresponding author: bcunning@illinois.edu

Received 19 June 2009; revised 17 October 2009; accepted 2 November 2009;
posted 3 November 2009 (Doc. ID 112892); published 20 November 2009

A theory is derived to describe the relationship between photonic crystal (PC) label-free imaging resolution and PC resonance spectral linewidth and location. PCs are fabricated and patterned with a resolution standard photomask in order to verify this relationship experimentally. Two distinct linear resolutions of $<1\,\mu$m and $3.5\,\mu$m are demonstrated in orthogonal directions on a single device, where the former is limited by the imaging system optics and the latter is constrained by finite resonant mode propagation. In order to illustrate the utility of improved design control, the spectral response of a PC is optimized for label-free imaging of immobilized DNA capture spots on a microarray.

OCIS codes: 280.1415, 050.5298, 108.0180.

1. Introduction

The rapid development of new biomolecular techniques over the past several decades has created a need for complementary technologies to accurately detect, measure, and characterize these systems in biomedical research and diagnostics applications. One important class of devices that are finding wide-ranging applications in this arena is label-free biosensors. In particular, there has been an exceptional research effort into label-free optical sensors that are capable of monitoring the binding affinity, specificity, and kinetics of biomolecular interactions. Labels employing fluorescence, dyes, or radioisotopes have traditionally been used for this purpose, but these have the disadvantage of potentially modifying analyte conformation, blocking binding sites, inducing steric hindrance, and in the case of fluorescent tags, bleaching very quickly and being subject to quenching. Furthermore, it can be extremely time consuming and costly to find an appropriate label that functions uniformly across a system of interest. Label-free detection can be instrumental in overcoming the cost, complexity, and uncertainty of biomolecular detection using traditional tags [1].

Optical biosensors generally use evanescent fields to probe the optical properties of a region containing an analyte. This near-surface detection scheme is ideal for monitoring biochemical interactions involving proteins, cells, nucleic acids, or other biomolecules at a surface while minimizing the contribution of bulk solution effects. Numerous optical sensing modalities have been demonstrated, but only a few are amenable to formats that enable highly multiplexed analysis or imaging of a sensor surface. Such capabilities are essential for adoption of optical biosensing technology for high-throughput screening in pharmaceutical development, personal genomics, and molecular diagnostics [2,3]. Both surface plasmon resonance and ellipsometry have shown promising recent results for sensitive label-free

0003-6935/09/346567-08$15.00/0

optical imaging [4–6]. A third approach using photonic crystal (PC) surfaces has been applied successfully to numerous applications in life science research, pharmaceutical drug discovery, and environmental monitoring [7–9]. This biosensor structure is a one-dimensional surface PC comprised of a low refractive index linear grating surface structure coated with a high refractive index film. The sensors can be fabricated over large areas by means of nanoreplication and incorporated into standard 96- and 384-well microplates or on to glass microscope slides. The PCs used for label-free biodetection support a spectrally narrow resonant reflection peak with near 100% efficiency [10]. Surface-based label-free sensing is achieved by monitoring changes in the wavelength (at a fixed incident angle) or angle (at a fixed incident wavelength) of this resonance as biological material with dielectric permittivity greater than the surrounding medium (usually water or air) is adsorbed to the device surface. Due to the spatially localized nature of these resonances in the plane of the PC surface, label-free imaging can be performed by mapping the spatial distribution of resonance conditions across an area of the PC. Using an instrument capable of pixel resolutions as small as $6\,\mu\mathrm{m} \times 6\,\mu\mathrm{m}$, label-free imaging has been demonstrated for multiplexed spot-based protein assays [11,12], the determination of protein–protein kinetics within microfluidic networks [13], cell-surface characterization, and viability monitoring [14,15].

The primary advantages of this technology are the low device fabrication cost, the ease with which the structures can be adapted to standardized formats, the spectrally narrow resonances and high sensitivity, and the ability to perform highly multiplexed analysis and label-free imaging. While the potential for PC label-free sensing is clear, there has yet to be a thorough investigation into the resolution limitations resulting from the finite propagation length of resonant modes along the photonic crystal. As the prospective applications of this technique are dictated by the achievable resolution, we seek here to predict, control, and characterize the inherent resolution of PC label-free imaging. We first present a theory for predicting PC label-free imaging resolution based on the propagation length of resonant modes. Subsequently we employ a recently developed microscope-based label-free imaging system to experimentally characterize the spatial resolution of PCs patterned with a resolution standard photomask. Finally, we demonstrate control of the spatial resolution by tuning the PC resonance properties, and with this capability we engineer devices for improved label-free imaging of micrometer-scale diameter spots of biomolecular capture probes.

2. Photonic Crystal Resonance Theory

PCs used for label-free sensing are composed of a low-refractive index linear surface-relief grating coated with a thin high-refractive index guidance layer. The grating structure enables coupling of external illumination at particular wavelength and incidence angle combinations through phase matching to "leaky" modes supported by the effective high-index layer. A leaky mode refers to light that is weakly guided along the high-index layer, as the grating provides not only efficient in-coupling, but also out-coupling. Using ray tracing arguments, it can be shown that the out-coupled light constructively interferes with specular reflected light while destructively interfering with directly transmitted light [10]. The result is 100% reflection efficiency at this particular incidence angle and wavelength with a Lorentzian lineshape about this point [16]. This highly efficient resonance takes advantage of the inability of the subwavelength-period grating to diffract real propagating modes for all but the 0th reflected and transmitted orders. Instead, the evanescent ± 1 order modes couple energy into and out of the device.

The phase matching condition for in-coupling light to a resonant mode is given by

$$k_0 \sin(\theta_0) \pm m\frac{2\pi}{\Lambda} = \frac{2\pi}{\lambda} n_{\mathrm{eff}}, \tag{1}$$

where k_0 is the free-space wave number, θ_0 is the resonance angle measured from the normal, m is the diffraction order, Λ is the grating period, λ is the resonance wavelength, and n_{eff} is the effective index of the resonant mode. Equation (1) shows how one can vary the illumination angle, wavelength, or both to excite a PC resonance. For illumination close to the normal, Eq. (1) can be approximated by

$$\lambda = \Lambda n_{\mathrm{eff}}. \tag{2}$$

The PC stores optical energy at resonance through confinement within a thin high-index region at the device surface. Energy loss from the resonator occurs as the grating leaks light to externally propagating modes, the rate at which determines the lateral energy confinement. The propagation length of a resonant leaky mode of known spectral width and center wavelength can be determined by first computing the photon lifetime in this resonator,

$$\tau_p = \frac{Q}{\omega_0} = \frac{\lambda^2 n_{\mathrm{eff}}}{2\pi \cdot \Delta\lambda \cdot c}, \tag{3}$$

where Q is the resonator quality (Q) factor, $\Delta\lambda$ is the spectral width of the resonance, and all other symbols are as previously defined. Using this definition, the photon lifetime is defined as the time where the probability that a resonant photon has yet to be diffracted into the far field is $1/e$ [17]. The propagation length, or the distance at which $1/e$ of the resonant photons remain in the mode, can then simply be computed by

$$L_p = \tau_p \cdot \frac{c}{n_{\mathrm{eff}}} = \frac{\lambda^2}{2\pi \cdot \Delta\lambda}. \tag{4}$$

Since λ is primarily determined by practical constraints such as the cost and availability of PC fabrication methods [λ is proportional to Λ by Eq. (2)] and illumination sources and detectors, L_p is therefore most easily controlled by modifying $\Delta\lambda$. The spectral width can be tuned based on the "modulation strength" of the grating, a combination of the grating depth and its refractive index contrast [18].

Equation (4) represents an uncertainty relationship between spectral and spatial precision. The uncertainty in propagation length will directly lead to uncertainty in the spatial distribution of resonant angles measured across a PC surface. Therefore, one can predict label-free imaging spatial resolution from this simple expression for leaky-mode propagation length, assuming resolution is not limited by the optical imaging system or by the signal magnitude relative to background noise. In the following sections we experimentally verify the relationship between resonance linewidth and label-free imaging resolution, investigate the limitations and the more precise origin of the label-free image, and demonstrate how careful control over device design is critical for optimizing label-free imaging in biological applications.

3. Photonic Crystal Label-Free Imaging

Accurate characterization of the inherent resolution limitations of PC label-free imaging mandates an imaging setup with sufficient optical resolution. Recently we have developed a microscope-based system that is capable of high-resolution imaging of resonance shifts due to biomolecular adsorption and is designed such that these label-free images can be self-registered to bright field and fluorescence images [19]. In contrast to previous wavelength-based reflection detection schemes, this instrument monitors the resonance condition as a function of illumination angle for a fixed laser wavelength. The resonance angle measured at each pixel in the image can be correlated to the local adsorbed biomolecular density on the surface. The upright fluorescence microscope employed for the detection optics is capable of providing excellent diffraction-limited performance. However, the resolution of the label-free PC image can be further limited by the propagation of the resonant modes that give rise to the label-free image.

A schematic of the label-free imaging system used in this study is shown in Fig. 1(a), and a detailed description of the instrument and its operation has been given previously [19]. In brief, the laser source is a 35 mW helium–neon laser, the output of which passes through a waveplate for polarization control, a neutral density filter, a rotating ground-glass diffuser to reduce the beam's spatial coherence thereby limiting speckle and fringes at the imaging plane, a 10× beam expander to provide more uniform illumination, and an aperture for controlling the spatial extent of the beam. The remainder of the beam path makes use of an upright fluorescence microscope (Olympus BX-51) and an electron-multiplier charge coupled device (EM-CCD, Hamamatsu). Label-free detection is achieved by imaging laser transmission through a PC as a function of the laser incidence angle. The incidence angle is computer controlled and finely scanned about the expected resonance locations. The transmission versus angle data is fit on a pixel-by-pixel basis, and a label-free image is constructed where each pixel takes on the fitted value for the angle of minimum transmission. Figure 1(b) illustrates a PC resonance captured on a single pixel using single-wavelength variable-incidence-angle illumination. The CCD used for detection has 16 μm×16 μm pixels across an 8 mm×8 mm area. Appropriate magnification (indicated for each image) is used throughout this work to ensure the label-free response is imaged at significantly finer pixel resolution than the spatial Nyquist rate.

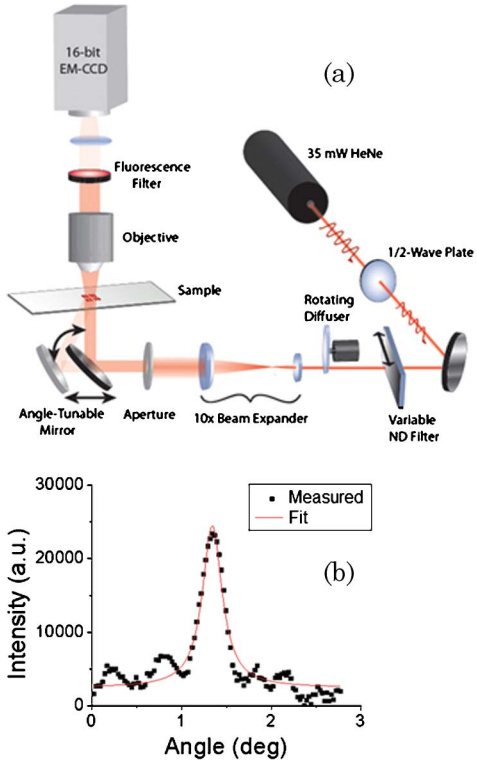

Fig. 1. (Color online) (a) Label-free imaging instrument schematic, reprinted from [19], and (b) sample measured inverted transmission versus angle resonance profile.

A schematic of the PC structure used throughout this work is shown in Fig. 2. The device is fabricated on a flexible plastic substrate using a nanoreplication process developed previously [20]. The replica molding approach enables low-cost, high-fidelity pattern transfer for large-area device fabrication. Briefly, the process involves first molding a thin layer of UV-curable epoxy (UVCP) with a silicon "master" wafer that has a negative image of the desired structure etched into the surface by deep-UV lithography and reactive ion etching. A UV cross-linking step followed by separation of the replica from the silane-functionalized silicon wafer yields the desired periodic structure on the plastic substrate. Thermal

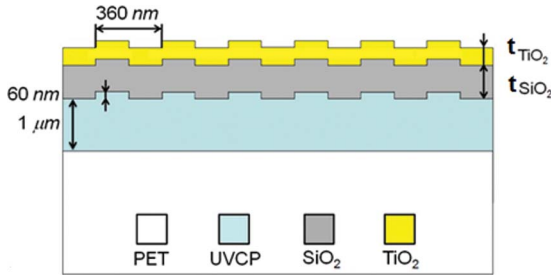

Fig. 2. (Color online) Schematic of photonic crystal structure designed for label-free and enhanced-fluorescence imaging. Adapted from [19].

evaporation or sputtering of the oxides completes the optical structure. For mechanical stability, 25 mm× 75 mm sections of the device are then affixed to standard glass microscope slides using an optical adhesive.

To characterize the resolution of PC label-free imaging, a photoresist layer (Shipley S-1805) spun onto a PC coated with 200 nm of TiO_2 and no SiO_2 layer was patterned with a USAF 1951 resolution standard photomask. The period of the grating ($L = 360$ nm) and the thickness of the TiO_2 were chosen in order to maximize label-free sensitivity while ensuring spectral overlap with the excitation source (He–Ne laser) near normal incidence. A rigorous study on optimizing the sensitivity of label-free PC biosensors has been given previously [21]. The photoresist layer provides a local refractive index change analogous to that for surface-based label-free biomolecular sensing and induces a local shift to a higher resonance angle. Bright field and label-free images were captured and are given in Figs. 3(a) and 3(b), respectively. The numbers by each line set correspond to line cycles/mm. Bright field imaging achieves submicron resolution for line pairs in either of the two orthogonal directions, ensuring that the optical system is not the limiting factor for subsequent label-free measurements. Label-free imaging demonstrates a clear directional effect in achievable resolution, as submicron resolution is demonstrated in the horizontal direction, while it is significantly blurred out in the vertical direction. The asymmetric resolution is the result of finite and unidirectional leaky-mode propagation in the direction parallel to the photonic crystal modulation, which is in the vertical direction in these images.

Label-free resolution is defined here as the separation distance between the edges of line pairs, where the oscillation magnitude of the label-free response across the lines and interceding spaces falls to $1/e$ that of larger "bulk" features. This method is illustrated in Fig. 3(c) by taking a line profile through a large feature with dimensions much greater than the anticipated label-free resolution and another profile across the finely spaced line pairs of the resolution pattern. As the line pairs become more finely spaced, the oscillations in the resonance angle become smaller and approach the average value between the resonance angle on the bulk photoresist pattern and off. This resolution definition is similar in nature to the Rayleigh and Sparrow criteria in that it defines a minimum spacing of the physical features below which the response functions (here a resonance angle rather than intensity point spread function) cannot be discerned as separate from one another. This minimum line spacing in this case is measured to be 3.5 μm in the vertical direction. Using a collimated white light source, a polarizer and a visible spectrometer (Ocean Optics), the spectral linewidth of the PC was measured to be 15 nm. Equation (4) can then be used to predict the resolution (approximated as the propagation length) as 4.3 μm for this resonance centered at 633 nm.

To illustrate the relationship between PC resonant linewidth and label-free imaging resolution, two devices with widely divergent resonant spectral linewidths were patterned with the same USAF 1951 resolution standard. Modifying the spectral linewidth can be accomplished by adjusting the thickness of a SiO_2 layer that sits below the high refractive index TiO_2 layer. Increasing the thickness of the SiO_2 coating directly affects the modulation strength of the PC by smoothing the surface profile, thereby reducing the resonance linewidth. The addition of SiO_2 has minimal impact on the effective index of the resonant mode, and so by Eq. (2) there

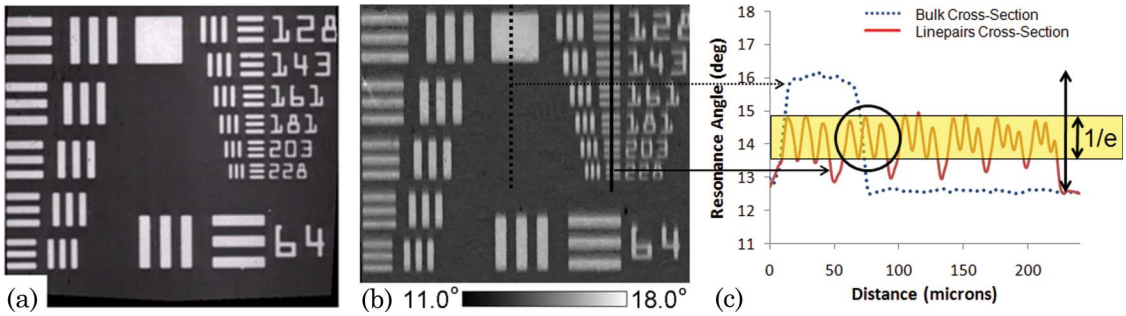

Fig. 3. (Color online) (a) Bright field and (b) label-free images of USAF 1951 resolution standard patterned into a photoresist by photolithography on a photonic crystal. Numbers define line pair cycles/mm, and the images are taken at 32× magnification. (c) Cross-section profile of line pairs and bulk feature to illustrate method for determining resolution, defined as the line spacing where the line pair label-free response is down by $1/e$ from that of the bulk.

is little influence on the resonance spectral location. In contrast to the data presented previously, the devices used here have the resolution pattern etched into the structure using reactive ion etching to a depth of 15 nm. The photoresist pattern had to be transferred directly into the structure because the resist imparted too high of an optical loss for the higher Q device. The two devices have measured linewidths of 17 nm (no SiO_2 coating, 200 nm TiO_2) and 4.5 nm (450 nm SiO_2 layer, 200 nm TiO_2), as shown in Fig. 4(a), and using Eq. (4) have predicted label-free resolutions of 3.7 μm and 14 μm, respectively. Label-free images captured for the broad and narrow-linewidth resolution test devices are given in Figs. 4(b) and 4(c) and the resolution is measured at 3.9 μm and 11 μm, respectively. Negative shifts of the resonance angle exist in regions that have been etched back to a depth of 15 nm.

The theory presented previously to calculate the propagation length of resonant photons provides a simple and tractable method for understanding the fundamental origins of label-free resolution limitations. The label-free images of resolution standards patterned onto several devices presented so far has aimed to confirm this theory. However, one can gain further insight by studying the evolution of resonant spectra gathered from several individual pixels across an effective index interface. Figure 5(b) shows a rotated section of the square feature present in the upper left-hand corner of Fig. 4(c). Figures 5(a) and 5(c) show inverted transmission versus angle responses for the resonances at pixels far away from the physical interface where part of the structure has been etched back. Away from the interface, the resonances appear as we would expect them. However, resonance profiles gathered from pixels near the interface are more complex, as shown in Figs. 5(d)–5(f). There are a couple of important observations to be made regarding the evolution of the local resonance across the interface. First, there is asymmetry about the interface due to the propagation direction of the leaky modes; in this case it is from right to left. Second, the data fitting is robust, and, at least for the case of this simple single interface, helps to accurately locate the true physical interface with significantly greater accuracy than might be predicted from Eq. (4). However, as in the case of more traditional optical resolution tests, accurately locating one point or line is not typically the challenge at hand for label-free biomolecular imaging but rather distinguishing adjacent features from one another. For this reason the resolution is characterized as defined previously and not for a single isolated feature edge.

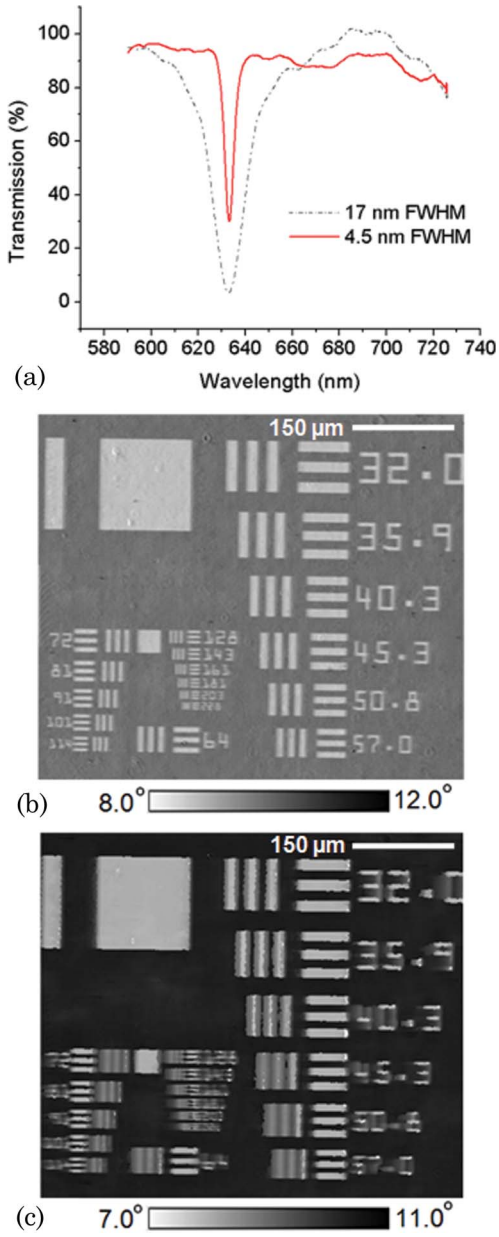

Fig. 4. (Color online) (a) Transmission versus wavelength resonance spectra for two photonic crystals. Label-free images of USAF 1951 resolution standard patterned etched into the photonic crystals with (b) broad and (c) narrow spectral linewidths. Numbers define line pair cycles/mm, and images were captured at 12.5× magnification.

4. Application to DNA Microarrays

The theoretical and empirical results presented in this work enable PCs to be engineered to a particular spatial resolution specification. A broader resonant linewidth has been demonstrated to improve spatial resolution. However, the wider spectral feature reduces the accuracy with which changes in the resonance location can be tracked [22]. Therefore, label-free resonant shift detection performance is sacrificed for spatial resolution. Given this trade-off, the particular label-free biosensing application must be considered when choosing the optimal PC design. To illustrate this concept, we perform label-free imaging of DNA microarray capture spots with two distinct PCs.

Microarrays printed by pin, inkjet, or piezoelectric spotting methods are prone to high variability of the density, size, and shape of immobilized capture DNA

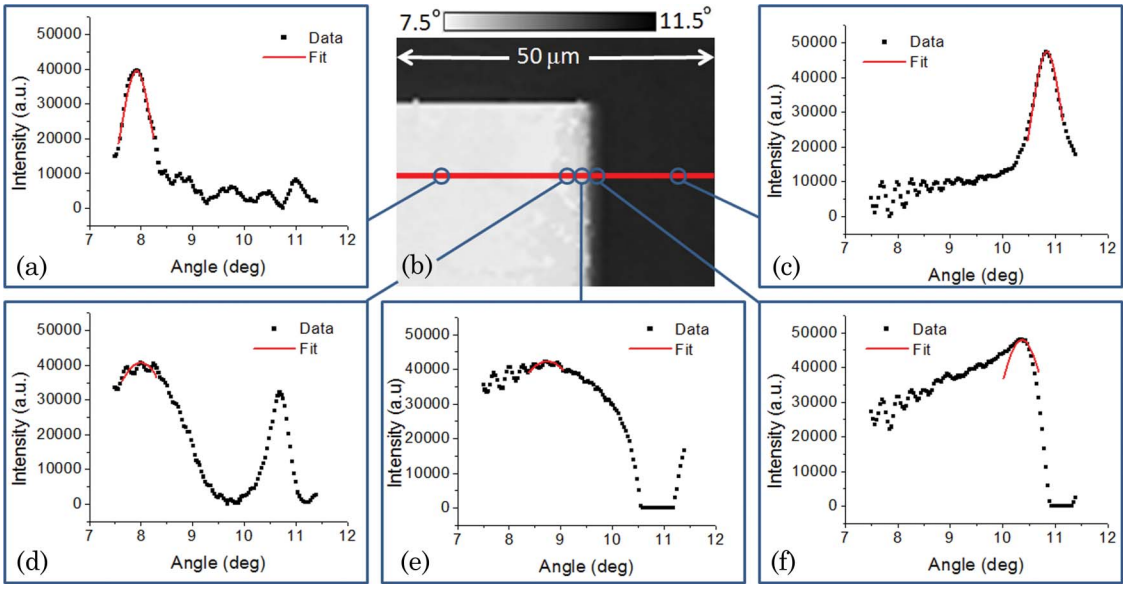

Fig. 5. (Color online) (b) Feature edge for resolution standard etched to a depth of 15 nm into the surface of the 4.5 nm linewidth PC. (a), (c)–(f) Inverted transmission versus angle responses and fitted peaks for pixels across the feature boundary and parallel to the direction of leaky mode propagation (right to left).

[23]. Since these variables influence hybridization kinetics [24,25], accounting for them can potentially lead to more accurate and reliable microarray results for disease research and diagnostics. Here we used a microarray containing 192 different 70 mer oligonucleotide sequences representative of known *Glycine max* genes. Prior to microarray printing, each PC was functionalized with (3-glycidoxypropyl)trimethoxysilane in vapor phase for 12 h. Using a *Q*Array^2 (Genetix) contact pin-spotter, slides were spotted with 40 replicates per oligo for a total of 7680 spots on a single slide. After spotting, the array was dried down at room temperature to facilitate surface binding, UV cross-linked, and subsequently washed in 0.1% sodium dodecyl sulfate (SDS) and dH$_2$O before imaging.

Figure 6(a) shows an inverted transmission versus angle response for the structure given in Fig. 2 with 300 nm of SiO_2 and 150 nm of TiO_2. A label-free image of the spotted array is given in Fig. 6(b), and an enlarged view of four spots is shown in Fig. 6(c). With the goal of improving the resolution of microarray capture spot imaging, a second PC was fabricated with a twofold broader resonant linewidth. This PC was fabricated with 20 nm more TiO_2 such that the resonance is located very close to normal incidence. The resonance broadens as it approaches normal incidence due to band bending of the photonic crystal dispersion. The deposition of additional TiO_2 also tends to slightly broaden the resonance, as this extra material effectively increases the grating strength. While modulating the thickness of the SiO_2 layer is an easier method for controlling the resonance linewidth, this technique enables equivalent results. Resonances close to normal incidence were not used for the resolution standard study described previously since the large resonance shifts induced by the photoresist or etching could result in aliasing of the signal across zero degrees due to symmetry of the photonic crystal dispersion. The angular response for the second device is given in Fig. 6(d), and label-free images of the same area of the identical array spotted on to this device are shown in Figs. 6(e) and 6(f). The physical perimeter of the spots is significantly clearer for the broader resonance linewidth device, enabling more accurate boundary determination for the microarray analysis software (GenePix Pro, Molecular Devices). This is crucial in order to ensure density information is collected from the spots themselves and is not influenced by contributions from the adjacent background signal. The trade-off for this improved spatial resolution is a reduction in the signal-to-noise ratio (SNR) of the label-free image. SNR is defined as the background subtracted label-free spot signal divided by the standard deviation of the background (the noise) and is directly related to the detection limit of the label-free imaging technique. The background is measured locally for each spot as the corners around the spot. The average SNR for the 100 spots imaged on the narrow and broad linewidth devices is calculated to be 24.6 ± 7.6 and 18.5 ± 4.7, respectively. This change in the SNR agrees well with theory, predicting a scaling factor of $\mathrm{FWHM}_n^{(1/2)}/\mathrm{FWHM}_b^{(1/2)}$, where $\mathrm{FWHM}_{n,b}$ represents the full width at half-maximum of the narrow and broad resonances, respectively [22]. Given the large label-free resonance shift magnitudes of the microarray spots, this small reduction in SNR for the near-normal incidence PC does not significantly affect the ability to resolve spot density differences. Further spatial resolution improvements are not necessary for this application,

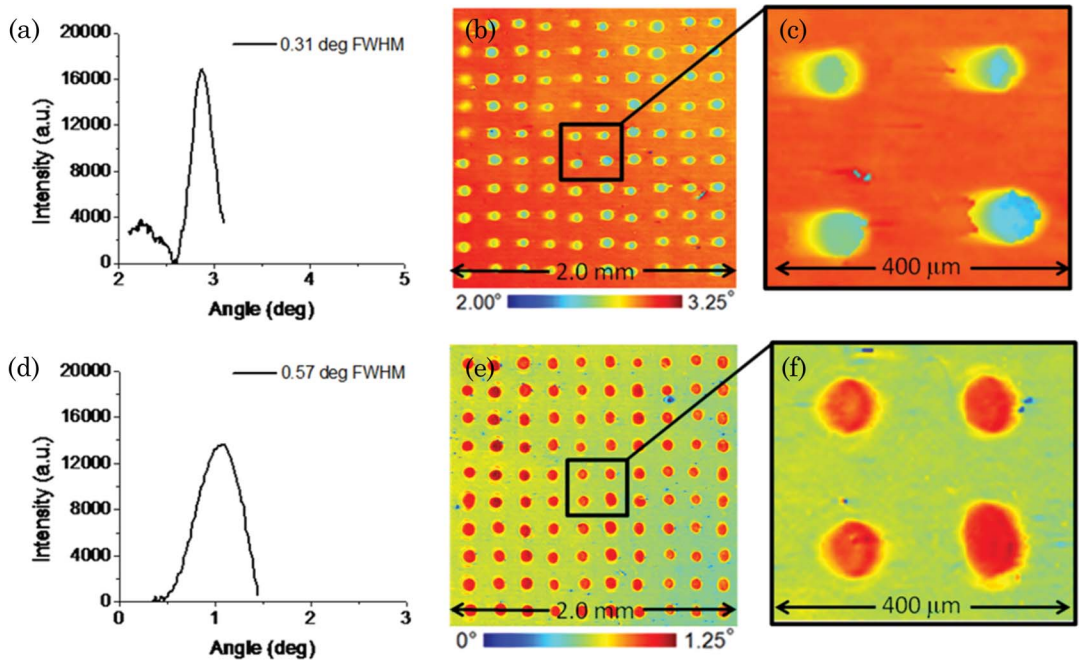

Fig. 6. (Color online) (a) Inverted transmission versus angle response for a PC with 300 nm SiO_2 and 150 nm and (b), (c) label-free images of this PC with DNA capture probes printed onto the device in a microarray format. (d) Inverted transmission versus angle response for a PC with 300 nm SiO_2 and 170 nm TiO_2 and (e), (f) label-free images of this PC with DNA capture probes printed onto the device in a microarray format.

and so we find this broader resonance linewidth PC to be more optimal in this particular scenario.

An additional factor in determining label-free imaging SNR is the size of the spots being imaged. A larger spot yields an increased number of samples (pixels), and so theoretically the detection limit will be inversely proportional to the square root of the sample size. Practical limitations such as device and spotting defects and nonuniformities that skew the distribution will, however, ultimately limit this value. In the case of DNA microarrays, spot sizes are chosen in order to maximize array density while maintaining sufficient optical sampling of the fluorescence emitted by each spot. It is therefore not practical to modify the geometry of the spots for the purpose of label-free quality control.

Although we have demonstrated optimization of the imaging resolution for a PC used for DNA microarray quality control, the results presented in this work should enable the design of PCs for other applications. For example, a more extreme change to the PC could be useful in the case of label-free cellular imaging. Eukaryotic cells are typically on the order of 10 μm in size, and so a very broad linewidth would be needed to accurately resolve cellular morphology. An example of an application requiring as narrow a resonance as possible would be label-free detection of protein disease biomarkers. Array density for protein detection is generally less of a concern; therefore the immobilized spots of capture antibody to the protein of interest could be enlarged. This will increase the optical sample size while also limiting the resolution requirements in exchange for better label-free spectral resolution, both yielding higher SNR and consequently a reduced detection limit.

5. Conclusions

PC label-free imaging resolution is dictated by resonant leaky-mode propagation, where a simple relation has been derived to relate the propagation length with the resonance spectral width and center wavelength. PCs fabricated with varying resonance linewidths and patterned with a resolution standard photomask have been used to demonstrate good agreement with this theory. Furthermore, asymmetry in the achievable label-free imaging resolution has been investigated, where resolution is measured down to submicron and 3.5 μm in the directions perpendicular and parallel to, respectively, the direction of leaky-mode propagation. Finally, by careful tuning of the PC spectral characteristics, the label-free imaging quality of capture spots of a DNA microarray printed on a PC has been optimized.

This work was supported by SRU Biosystems, the National Science Foundation (NSF) (CBET 07-54122), and the National Institutes of Health (NIH) (PHS 1 R01 CA118562). Any opinions, findings, and conclusions or recommendations expressed in this material are those of the authors and do not necessarily reflect the views of the National Science Foundation.

References

1. A. J. Cunningham, *Introduction to Bioanalytical Sensors* (Wiley-Interscience, 1998).
2. M. Schena, *Microarray Analysis* (Wiley-Liss, 2002).

3. H. Zhu, M. Bilgin, R. Bangham, D. Hall, A. Casamayor, P. Bertone, N. Lan, R. Jansen, S. Bidlingmaier, T. Houfek, T. Mitchell, P. Miller, R. A. Dean, M. Gerstein, and M. Snyder, "Global analysis of protein activities using proteome chips," Science **293**, 2101–2105 (2001).
4. J. S. Shumaker-Parry and C. T. Campbell, "Quantitative methods for spatially resolved adsorption/desorption measurements in real time by surface plasmon resonance microscopy," Anal. Chem. **76**, 907–917 (2004).
5. X. Zhu, J. P. Landry, Y.-S. Sun, J. P. Gregg, K. S. Lam, and X. Guo, "Oblique-incidence reflectivity difference microscope for label-free high-throughput detection of biochemical reactions in a microarray format," Appl. Opt. **46**, 1890–1895 (2007).
6. E. Ozkumur, J. W. Needham, D. A. Bergstein, R. Gonzalez, M. Cabodi, J. M. Gershoni, B. B. Goldberg, and M. S. Unlu, "Label-free and dynamic detection of biomolecular interactions for high-throughput microarray applications," Proc. Natl. Acad. Sci. USA **105**, 7988–7992 (2008).
7. P. C. Mathias, N. Ganesh, L. L. Chan, and B. T. Cunningham, "Label-free assays on the BIND system," J. Biomol. Screen. **9**, 481–490 (2004).
8. L. L. Chan, M. F. Pineda, J. Heeres, P. Hergenrother, and B. T. Cunningham, "General method for discovering inhibitors of protein-DNA interactions using photonic crystal biosensors," ACS Chem. Biol. **3**, 437–448 (2008).
9. M. F. Pineda, L. L. Chan, T. Kuhlenschmidt, M. Kuhlenschmidt, and B. T. Cunningham, "Rapid label-free selective detection of porcine rotavirus using photonic crystal biosensors for groundwater monitoring," IEEE Sens. J. **9**, 470–477 (2009).
10. D. Rosenblatt, A. Sharon and A. A. Friesem, "Resonant grating waveguide structures," IEEE J. Quantum Electron. **33**, 2038–2059 (1997).
11. P. Li, B. Lin, J. Gerstenmaier, and B. T. Cunningham, "A new method for label-free imaging of biomolecular interactions," Sens. Actuators B **99**, 6–13 (2004).
12. L. L. Chan, P. Y. Li, D. Puff, and B. T. Cunningham, "A self-referencing method for microplate label-free photonic crystal biosensors," IEEE Sens. J. **6**, 1551–1556 (2006).
13. C. J. Choi and B. T. Cunningham, "A 96-well microplate incorporating a replica molded microfluidic network integrated with photonic crystal biosensors for high throughput kinetic biomolecular interaction analysis," Lab Chip **7**, 550–556 (2007).
14. L. Chan, S. Gosangari, K. Watkin, and B. T. Cunningham, "A label-free photonic crystal biosensor imaging method for detection of cancer cell cytotoxicity and proliferation," Apoptosis **12**, 1061–1068 (2007).
15. L. L. Chan, S. Gosangari, K. L. Watkin, and B. T. Cunningham, "Label-free imaging of cancer cells using photonic crystal biosensors and application to cytotoxicity screening of a natural compound library," Sens. Actuators B **132**, 418–425 (2008).
16. S. Fan and J. D. Joannopoulos, "Analysis of guided resonances in photonic crystal slabs," Phys. Rev. B **65**, 235112 (2002).
17. J. Verdeyen, *Laser Electronics* (Prentice-Hall, 1995).
18. Y. Ding and R. Magnusson, "Resonant leaky-mode spectral-band engineering and device applications," Opt. Express **12**, 5661–5674 (2004).
19. I. D. Block, P. C. Mathias, N. Ganesh, S. Jones, B. R. Dorvel, V. Chaudhery, L. Vodkin, R. Bashir, and B. T. Cunningham, "A detection instrument for enhanced-fluorescence and label-free imaging on photonic crystal surfaces," Opt. Express **17**, 13222–13235 (2009).
20. B. T. Cunningham, B. Lin, J. Qiu, P. Li, J. Pepper, and B. Hugh, "A plastic colorimetric resonant optical biosensor for multiparallel detection of label-free biochemical interactions," Sens. Actuators B **85**, 219–226 (2002).
21. I. D. Block, N. Ganesh, M. Lu, and B. T. Cunningham, "A sensitivity model for predicting photonic crystal biosensor performance," IEEE Sens. J. **8**, 274–280 (2008).
22. W. C. Karl and H. H. Pien, "High-resolution biosensor spectral peak shift estimation," IEEE Trans. Signal Process. **53**, 4631–4639 (2005).
23. R. Auburn, D. P. Kreil, L. A. Meadows, B. Fischer, S. S. Matilla, and S. Russell, "Robotic spotting of cDNA arrays and oligonucleotide microarrays," Trends Biotechnol. **23**, 374–379 (2005).
24. A. W. Peterson, R. J. Heaton, and R. M. Georgiadis, "The effect of surface probe density on DNA hybridization," Nucleic Acids Res. **29**, 5163–5168 (2001).
25. D. S. Dandy, P. Wu, and D. W. Grainger, "Array feature size influences nucleic acid surface capture in DNA microarrays," Proc. Natl. Acad. Sci. USA **104**, 8223–8228 (2007).